Shunts vs. networks: tuning and comparison of passive centralized and decentralized piezoelectric vibration absorbers - supplementary materials

Ghislain Raze, Jennifer Dietrich, Boris Lossouarn and Gaëtan Kerschen

May 2022

1 Introduction

The purpose of this document is to present a refined version of the tuning procedure for a set of digital vibration absorbers (DVAs) proposed in the article "*Shunts vs. networks: tuning and comparison of passive centralized and decentralized piezoelectric vibration absorbers*". Specifically, this refined tuning procedure brings corrections to the electrical resonance frequency and damping matrices in order to account for the effect of non-resonant modes [1] (including the non-block diagonal character of the matrix $\mathbf{D}$) and sampling delays [2]. Details about the DVAs used in the experiments are also given.

This document is organized as follows. Section 2 briefly reviews the dynamics of the electromechanical system. The refined tuning procedure is then presented in Section 3. Finally, Section 4 presents the electrical circuit of the DVAs used in this work.

2 Dynamics of a piezoelectric structure connected to a set of DVAs

The governing equations of a piezoelectric structure coupled to a set of DVAs are recalled here for completeness. For the host system, they are given by

$$\begin{cases} \left(s^2\mathbf{I} + \boldsymbol{\Omega}_{oc}^2\right)\boldsymbol{\eta}_{oc} - \dfrac{1}{s}\mathbf{B}\mathbf{V}_{out} = \boldsymbol{\Phi}_{oc}^T\mathbf{f} \\ \mathbf{C}\boldsymbol{\eta}_{oc} - \dfrac{1}{s}\mathbf{D}\mathbf{V}_{out} = \mathbf{V}_{in} \end{cases}, \tag{1}$$

where s is Laplace's variable, $\mathbf{I}$ is the identity matrix, $\boldsymbol{\Omega}_{oc}^2$ is a diagonal matrix containing the squared resonance frequencies of the structure with open-circuited patches, $\boldsymbol{\eta}_{oc}$ is a vector of open-circuit modal coordinates, $\boldsymbol{\Phi}_{oc}$ is the open-circuit mode shapes matrix, and

$$\mathbf{B} = \boldsymbol{\Theta}_\Phi\mathbf{G}_{out}, \qquad \mathbf{C} = \mathbf{G}_{in}\boldsymbol{\Theta}_\Phi^T, \qquad \mathbf{D} = \mathbf{G}_{in}\mathbf{E}_p^\varepsilon\mathbf{G}_{out}, \tag{2}$$

where $\mathbf{\Theta}_\Phi$ is a modal electromechanical coupling matrix, $\mathbf{G}_{in}$ and $\mathbf{G}_{out}$ are matrices representing the voltage sensors and current sources gains of the DVAs, respectively, and $\mathbf{E}_p^\varepsilon$ is the elastance matrix of the piezoelectric transducers at constant strain.

The DVAs are programmed to emulate a transfer function $\mathbf{Z}_{DVA}$ between the input and output of the digital unit as

$$\mathbf{V}_{in} = \mathbf{Z}_{DVA}(s)\mathbf{V}_{out}. \tag{3}$$

To provide effective multimodal control, this impedance matrix is sought to satisfy the following relation

$$\mathbf{\Phi}_{in}^T \left(\mathbf{D} + s\mathbf{Z}_{DVA}(s)\right) \mathbf{\Phi}_{out} = s^2\mathbf{\Omega}_e^{-2} + 2s\mathbf{Z}_e\mathbf{\Omega}_e^{-1} + \mathbf{I}, \tag{4}$$

where $\mathbf{\Phi}_{in}$ and $\mathbf{\Phi}_{out}$ are electrical input and output mode shapes matrices, respectively, and $\mathbf{\Omega}_e$ and $\mathbf{Z}_e$ are diagonal matrices containing the electrical resonance frequencies and damping ratios, respectively. Introducing the modal electrical coordinates $\boldsymbol{\eta}_e$ by

$$\frac{1}{s}\mathbf{V}_{out} = \mathbf{\Phi}_{out}\boldsymbol{\eta}_e \tag{5}$$

results in the following governing equations for the controlled system

$$\begin{cases} \left(s^2\mathbf{I} + \mathbf{\Omega}_{oc}^2\right)\boldsymbol{\eta}_{oc} - \mathbf{B}\mathbf{\Phi}_{out}\boldsymbol{\eta}_e = \mathbf{\Phi}_{oc}^T\mathbf{f} \\ \left(s^2\mathbf{\Omega}_e^{-2} + 2s\mathbf{Z}_e\mathbf{\Omega}_e^{-1} + \mathbf{I}\right)\boldsymbol{\eta}_e - \mathbf{\Phi}_{in}^T\mathbf{C}\boldsymbol{\eta}_{oc} = 0 \end{cases}. \tag{6}$$

It is also recalled that the electrical mode shapes satisfy the reciprocity condition

$$\mathbf{B}\mathbf{\Phi}_{out} = \mathbf{C}^T\mathbf{\Phi}_{in}. \tag{7}$$

2.1 Discussion on the block diagonal character of the matrix D

It is now assumed that the transducers and DVAs are grouped into N_g independent groups. Superscript (g) is used to denote the characteristics associated to group g ($g = 1, \cdots, N_g$).

A decentralized implementation is only possible if $\mathbf{D}$ itself has a block diagonal structure. It is reasonable to assume that $\mathbf{G}_{in}$ and $\mathbf{G}_{out}$ have the same block diagonal structure since the DVAs belonging to different groups are not supposed to interact directly with each other. Furthemore, the matrix $\mathbf{E}_p^\varepsilon$ of the full model should be diagonal. These two facts combined with the definition of $\mathbf{D}$ (Equation (2)) indeed result in a block diagonal matrix. $\mathbf{E}_p^\varepsilon$ might nonetheless not be diagonal when modes of higher frequency than the bandwidth of interest are condensed to account only for their static contribution [3]. This is the case, e.g., if a reduced-order model is used, or in experimental measurements in general. This non-diagonality can destroy the block diagonal structure of $\mathbf{D}$. However, these effects are generally small and can be neglected at first, and will be accounted for later as corrections when tuning the resonance frequencies and damping ratios of the networks. Hence, $\mathbf{D}$ can be decomposed into

$$\mathbf{D} = \mathbf{D}_{BD} + \mathbf{D}_{ND}, \tag{8}$$

where $\mathbf{D}_{BD}$ is a block diagonal matrix whose diagonal blocks are equal to those of $\mathbf{D}$, i.e.,

$$\mathbf{D}_{BD} = \mathbf{blkdiag}\left(\mathbf{D}^{(1)}\ ,\ \cdots\ ,\ \mathbf{D}^{(N_g)}\right), \tag{9}$$

where $\mathbf{D}^{(g)}$ is the restriction of $\mathbf{D}$ to the electrical degrees of freedom of group g. $\mathbf{D}_{ND}$ then contains the non-diagonal blocks (for a fully centralized network, $\mathbf{D} = \mathbf{D}^{(1)} = \mathbf{D}_{BD}$ and $\mathbf{D}_{ND} = \mathbf{0}$). The electrical mode shapes will be tuned ignoring the latter, i.e., setting them considering that Equation (4) is replaced by

$$\boldsymbol{\Phi}_{in}^T \left(\mathbf{D}_{BD} + s\mathbf{Z}_{DVA}(s)\right) \boldsymbol{\Phi}_{out} = s^2\boldsymbol{\Omega}_e^{-2} + 2s\mathbf{Z}_e\boldsymbol{\Omega}_e^{-1} + \mathbf{I}. \tag{10}$$

However, using Equations (1), (4), (5), (8) and (10), the actual system is found to be governed by the equations

$$\begin{cases} \left(s^2\mathbf{I} + \boldsymbol{\Omega}_{oc}^2\right)\boldsymbol{\eta}_{oc} - \mathbf{B}\boldsymbol{\Phi}_{out}\boldsymbol{\eta}_e = \boldsymbol{\Phi}_{oc}^T\mathbf{f} \\ \left(s^2\boldsymbol{\Omega}_e^{-2} + 2s\mathbf{Z}_e\boldsymbol{\Omega}_e^{-1} + \boldsymbol{\Delta}\right)\boldsymbol{\eta}_e - \boldsymbol{\Phi}_{in}^T\mathbf{C}\boldsymbol{\eta}_{oc} = 0 \end{cases}, \tag{11}$$

where

$$\boldsymbol{\Delta} = \mathbf{I} + \boldsymbol{\Phi}_{in}^T\mathbf{D}_{ND}\boldsymbol{\Phi}_{out} \tag{12}$$

is a non-necessarily diagonal matrix with small off-diagonal terms stemming from the neglected non-block diagonal part of $\mathbf{D}$. The influence of this non-ideal term can be accounted for when tuning the frequencies and damping ratios of the network.

2.2 Modal electromechanical coupling

The assessment procedure for the electromechanical coupling between resonant mechanical and electrical modes is recalled here. In Equation (6), a single mechanical resonant mode r and corresponding electrical resonant modes (distributed over the groups targeting that mode) indexed by $\mathbf{k}$ are considered, while every other mode is assumed to be quiescent. This leads to the reduced dynamical equations

$$\begin{cases} \left(s^2 + \omega_{oc,r}^2\right)\eta_{oc,r} - \mathbf{b}_r\boldsymbol{\Phi}_{out,\mathbf{k}}\boldsymbol{\eta}_{e,\mathbf{k}} = \boldsymbol{\phi}_{oc,r}^T\mathbf{f} \\ \left(s^2\boldsymbol{\Omega}_{e,\mathbf{k}}^{-2} + 2s\mathbf{Z}_{e,\mathbf{k}}\boldsymbol{\Omega}_{e,\mathbf{k}}^{-1} + \mathbf{I}\right)\boldsymbol{\eta}_{e,\mathbf{k}} - \boldsymbol{\Phi}_{in,\mathbf{k}}^T\mathbf{c}_r\eta_{oc,r} = 0 \end{cases}, \tag{13}$$

where $\mathbf{b}_r$ and $\mathbf{c}_r$ are the r^{th} line of $\mathbf{B}$ and column of $\mathbf{C}$, respectively. A modal electromechanical coupling factor (MEMCF) $\alpha_{c,r\mathbf{k}}$ can then be deduced as

$$\alpha_{c,r\mathbf{k}}^2 = \frac{1}{\omega_{oc,r}^2}\mathbf{b}_r\boldsymbol{\Phi}_{out,\mathbf{k}}\boldsymbol{\Phi}_{in,\mathbf{k}}^T\mathbf{c}_r. \tag{14}$$

3 Tuning of centralized and decentralized absorbers

The dynamics and coupling characteristics derived in the previous section are now exploited to tune the DVAs. Specifically, the electrical mode shapes, resonance frequencies and damping ratios are tuned to provide effective multimodal vibration mitigation of the controlled structure. The electrical mode shapes are first tailored to maximize the modal electromechanical coupling. The dynamics are then simplified to derive effective characteristics of the system around a specific resonance frequency. These characteristics can be corrected to account for the potential effect of the delays incurred by the sampling procedure of the digital unit. They are used to accurately tune the electrical resonance frequencies and damping ratios. Finally, the realization of the resulting shunt(s) and/or network(s) using DVAs is discussed.

3.1 Optimal input and output mode shapes

The expression of the optimal electrical mode shapes is recalled here for completeness. Let the singular value decomposition (SVD) of $\mathbf{D}^{(g)}$ be given by

$$\mathbf{D}^{(g)} = \mathbf{U}_D^{(g)} \mathbf{\Sigma}_D^{(g)} \left(\mathbf{V}_D^{(g)} \right)^T. \tag{15}$$

Modified input and output matrices are built as

$$\mathbf{B}^{(g)} \mathbf{V}_D^{(g)} \left(\mathbf{\Sigma}_D^{(g)} \right)^{-1/2} = \begin{bmatrix} \mathbf{b}_{D,1}^{(g)} \\ \vdots \\ \mathbf{b}_{D,N_e^{(g)}}^{(g)} \end{bmatrix}, \qquad \left(\mathbf{C}^{(g)} \right)^T \mathbf{U}_D^{(g)} \left(\mathbf{\Sigma}_D^{(g)} \right)^{-1/2} = \begin{bmatrix} \mathbf{c}_{D,1}^{(g)} \\ \vdots \\ \mathbf{c}_{D,N_e^{(g)}}^{(g)} \end{bmatrix}, \tag{16}$$

and a scaling matrix $\mathbf{S}^{(g)} = \mathbf{diag}\left(s_1^{(g)}, \cdots, s_{N_e^{(g)}}^{(g)} \right)$ whose elements are built from the rows of these modified input and output matrices as

$$s_k^{(g)} = \sqrt{\frac{||\mathbf{c}_{D,k}^{(g)}||}{||\mathbf{b}_{D,k}^{(g)}||}}, \qquad k \in [1, \cdots, N_e^{(g)}]. \tag{17}$$

Finally, given the compact SVD

$$\mathbf{S}^{(g)} \mathbf{W}^{(g)} \mathbf{\Omega}_{oc}^{-1} \mathbf{B}^{(g)} \mathbf{V}_D^{(g)} \left(\mathbf{\Sigma}_D^{(g)} \right)^{-1/2} = \mathbf{U}_M^{(g)} \mathbf{\Sigma}_M^{(g)} \left(\mathbf{V}_M^{(g)} \right)^T, \tag{18}$$

optimal input and output mode shapes are given by

$$\mathbf{\Phi}_{in}^{(g)} = \mathbf{U}_D^{(g)} \left(\mathbf{\Sigma}_D^{(g)} \right)^{-1/2} \mathbf{\Psi}^{(g)} \left(\mathbf{S}^{(g)} \right)^{-1} \tag{19}$$

and

$$\mathbf{\Phi}_{out}^{(g)} = \mathbf{V}_D^{(g)} \left(\mathbf{\Sigma}_D^{(g)} \right)^{-1/2} \mathbf{\Psi}^{(g)} \mathbf{S}^{(g)}, \tag{20}$$

respectively, with the optimal dimensionless electrical mode shape matrix

$$\mathbf{\Psi}^{(g)} = \mathbf{V}_M^{(g)} \left(\mathbf{U}_M^{(g)} \right)^T. \tag{21}$$

3.2 Effective characteristics

After setting the electrical mode shapes, the resonance frequencies and damping ratios remain to be tuned. To do so, the reduced model in Equation (13) can be complemented to account for the influence of non-resonant modes. In particular, accounting for a quasi-static contribution of higher-frequency modes has been shown to yield a more accurate tuning for shunts [1, 4] and networks [3], and this approach is adopted here. The non-block diagonal character of $\mathbf{D}$ can also be accounted for at this point.

Equation (11) is rewritten considering resonant mechanical (r) and electrical ($\mathbf{k}$) modes, as well as higher-frequency mechanical ($> r$) and electrical ($> k$) modes. The latter are assumed to respond statically, i.e., terms proportional to s and s^2

governing the dynamics of these modes are neglected. It is also assumed that the forcing effect on the non-resonant modes is negligible (in the vector $\boldsymbol{\Phi}_{oc}^T\mathbf{f}$, only the element associated to mode r, $\boldsymbol{\phi}_{oc,r}^T\mathbf{f}$, is assumed to be nonzero in the frequency range of interest)[1]. The simplified governing equations now read

$$\left(s^2 \left[\begin{array}{cc|cc} 1 & \mathbf{0} & \mathbf{0} & \mathbf{0} \\ \mathbf{0} & \boldsymbol{\Omega}_{e,\mathbf{k}}^{-2} & \mathbf{0} & \mathbf{0} \\ \hline \mathbf{0} & \mathbf{0} & \mathbf{0} & \mathbf{0} \\ \mathbf{0} & \mathbf{0} & \mathbf{0} & \mathbf{0} \end{array}\right] + s \left[\begin{array}{cc|cc} 0 & \mathbf{0} & \mathbf{0} & \mathbf{0} \\ \mathbf{0} & 2\mathbf{Z}_{e,\mathbf{k}}\boldsymbol{\Omega}_{e,\mathbf{k}}^{-1} & \mathbf{0} & \mathbf{0} \\ \hline \mathbf{0} & \mathbf{0} & \mathbf{0} & \mathbf{0} \\ \mathbf{0} & \mathbf{0} & \mathbf{0} & \mathbf{0} \end{array}\right] + \left[\begin{array}{cc|cc} \omega_{oc,r}^2 & -\mathbf{B}_r\boldsymbol{\Phi}_{out,\mathbf{k}} & \mathbf{0} & -\mathbf{B}_r\boldsymbol{\Phi}_{out,>k} \\ -\boldsymbol{\Phi}_{in,\mathbf{k}}^T\mathbf{C}_r & \boldsymbol{\Delta}_{\mathbf{kk}} & -\boldsymbol{\Phi}_{in,\mathbf{k}}^T\mathbf{C}_{>r} & \boldsymbol{\Delta}_{\mathbf{k}>k} \\ \hline \mathbf{0} & -\mathbf{B}_{>r}\boldsymbol{\Phi}_{out,\mathbf{k}} & \boldsymbol{\Omega}_{oc,>r}^2 & -\mathbf{B}_{>r}\boldsymbol{\Phi}_{out,>k} \\ -\boldsymbol{\Phi}_{in,>k}^T\mathbf{C}_r & \boldsymbol{\Delta}_{>k\mathbf{k}} & -\boldsymbol{\Phi}_{in,>k}^T\mathbf{C}_{>r} & \boldsymbol{\Delta}_{>k>k} \end{array}\right] \right) \left[\begin{array}{c} \eta_{oc,r} \\ \hline \boldsymbol{\eta}_{e,\mathbf{k}} \\ \boldsymbol{\eta}_{oc,>r} \\ \boldsymbol{\eta}_{e,>k} \end{array}\right] = \left[\begin{array}{c} \boldsymbol{\phi}_{oc,r}^T\mathbf{f} \\ \mathbf{0} \\ \mathbf{0} \\ \mathbf{0} \end{array}\right]. \tag{22}$$

For conciseness, this system is written with symmetric electromechanical mass, damping and stiffness matrices $\mathbf{M}^{EM}$, $\mathbf{C}^{EM}$ and $\mathbf{K}^{EM}$, respectively, partitioned as follows

$$\left(s^2 \left[\begin{array}{c|c} \mathbf{M}_{RR}^{EM} & \mathbf{0} \\ \hline \mathbf{0} & \mathbf{0} \end{array}\right] + s \left[\begin{array}{c|c} \mathbf{C}_{RR}^{EM} & \mathbf{0} \\ \hline \mathbf{0} & \mathbf{0} \end{array}\right] + \left[\begin{array}{c|c} \mathbf{K}_{RR}^{EM} & \mathbf{K}_{RB}^{EM} \\ \hline \mathbf{K}_{BR}^{EM} & \mathbf{K}_{BB}^{EM} \end{array}\right] \right) \left[\begin{array}{c} \eta_{oc,r} \\ \hline \boldsymbol{\eta}_{e,\mathbf{k}} \\ \boldsymbol{\eta}_{oc,>r} \\ \boldsymbol{\eta}_{e,>k} \end{array}\right] = \left[\begin{array}{c} \boldsymbol{\phi}_{oc,r}^T\mathbf{f} \\ \hline \mathbf{0} \\ \mathbf{0} \\ \mathbf{0} \end{array}\right], \tag{23}$$

where subscripts R and B are used to denote resonant and background electromechanical modes, respectively. From this equation, the higher-frequency modal coordinates can be expressed as functions of the resonant ones by

$$\left[\begin{array}{c} \boldsymbol{\eta}_{oc,>r} \\ \boldsymbol{\eta}_{e,>k} \end{array}\right] = -\left(\mathbf{K}_{BB}^{EM}\right)^{-1}\mathbf{K}_{BR}^{EM} \left[\begin{array}{c} \eta_{oc,r} \\ \boldsymbol{\eta}_{e,\mathbf{k}} \end{array}\right]. \tag{24}$$

Inserting this relation into the first lines of Equation (23) shows that the system is governed by

$$\left\{\begin{array}{l} \left(s^2 + \widehat{\omega}_{oc,r}^2\right)\eta_{oc,r} - \widehat{\mathbf{b}}_{r\mathbf{k}}\boldsymbol{\eta}_{e,\mathbf{k}} = \boldsymbol{\phi}_r^T\mathbf{f} \\ \left(s^2\boldsymbol{\Omega}_{e,\mathbf{k}}^{-2} + 2s\mathbf{Z}_{e,\mathbf{k}}\boldsymbol{\Omega}_{e,\mathbf{k}}^{-1} + \widehat{\boldsymbol{\Delta}}_{\mathbf{k}}\right)\boldsymbol{\eta}_{e,\mathbf{k}} - \widehat{\mathbf{c}}_{\mathbf{k}r}\eta_{oc,r} = \mathbf{0} \end{array}\right. \tag{25}$$

with the effective electromechanical stiffness matrix

$$\mathbf{K}_{RR}^{EM} - \mathbf{K}_{RB}^{EM}\left(\mathbf{K}_{BB}^{EM}\right)^{-1}\mathbf{K}_{BR}^{EM} = \left[\begin{array}{cc} \widehat{\omega}_{oc,r}^2 & -\widehat{\mathbf{b}}_{r\mathbf{k}} \\ -\widehat{\mathbf{c}}_{\mathbf{k}r} & \widehat{\boldsymbol{\Delta}}_{\mathbf{k}} \end{array}\right]. \tag{26}$$

[1]Taking the influence of external forcing in the tuning procedure more accurately is probably possible [5] but would be cumbersome.

The system in Equation (25) has the same form as that in Equation (13), but the effective characteristics in the former account for the influence of higher-frequency, non-resonant modes, making the tuning procedure more accurate. Nevertheless, since the matrix $\widehat{\mathbf{\Delta}}_{\mathbf{k}}$ is not diagonal, the electrical modal coordinates $\boldsymbol{\eta}_{e,\mathbf{k}}$ are coupled together.

Condensing the electrical response into the mechanical one, Equation (25) becomes

$$\left\{\left(s^2+\omega_{oc,r}^2\right)-\widehat{\mathbf{b}}_{r\mathbf{k}}\left(s^2\mathbf{\Omega}_{e,\mathbf{k}}^{-2}+2s\mathbf{Z}_{e,\mathbf{k}}\mathbf{\Omega}_{e,\mathbf{k}}^{-1}+\widehat{\mathbf{\Delta}}_{\mathbf{k}}\right)^{-1}\widehat{\mathbf{c}}_{\mathbf{k}r}\right\}\eta_{oc,r}=\mathbf{\Phi}_{oc,r}^T\mathbf{f}. \tag{27}$$

Since $\mathbf{\Omega}_{e,\mathbf{k}}$ and $\mathbf{Z}_{e,\mathbf{k}}$ are diagonal matrices, the coefficients of the latter can be chosen to ensure proportional damping. The effective electrical modes satisfying the equations

$$\widehat{\mathbf{\Delta}}_{\mathbf{k}}\widehat{\mathbf{\Phi}}_{e,\mathbf{k}}=\mathbf{\Omega}_{e,\mathbf{k}}^{-2}\widehat{\mathbf{\Phi}}_{e,\mathbf{k}}\widehat{\mathbf{\Omega}}_{e,\mathbf{k}}^2,\qquad \widehat{\mathbf{\Phi}}_{e,\mathbf{k}}^T\widehat{\mathbf{\Delta}}_{\mathbf{k}}\widehat{\mathbf{\Phi}}_{e,\mathbf{k}}=\mathbf{I} \tag{28}$$

can thus be used to express the response of this system through its modal expansion [6]

$$\left(s^2\mathbf{\Omega}_{e,\mathbf{k}}^{-2}+2s\mathbf{Z}_{e,\mathbf{k}}\mathbf{\Omega}_{e,\mathbf{k}}^{-1}+\widehat{\mathbf{\Delta}}_{\mathbf{k}}\right)^{-1}=\widehat{\mathbf{\Phi}}_{e,\mathbf{k}}\left(s^2\widehat{\mathbf{\Omega}}_{e,\mathbf{k}}^{-2}+2s\widehat{\mathbf{Z}}_{e,\mathbf{k}}\widehat{\mathbf{\Omega}}_{e,\mathbf{k}}^{-1}+\mathbf{I}\right)^{-1}\widehat{\mathbf{\Phi}}_{e,\mathbf{k}}^T, \tag{29}$$

where $\widehat{\mathbf{\Phi}}_{e,\mathbf{k}}$, $\widehat{\mathbf{\Omega}}_{e,\mathbf{k}}$ and $\widehat{\mathbf{Z}}_{e,\mathbf{k}}$ are the effective electrical mode shapes, resonance frequencies and damping matrices, respectively. From Equations (27) and (29), it is understood that the electromechanical coupling of these effective electrical modes is governed by the scalar product of the effective electrical mode shapes with $\widehat{\mathbf{c}}_{\mathbf{k}r}=\widehat{\mathbf{b}}_{r\mathbf{k}}^T$. The later vectors thus define an optimal direction that can be attributed to one of the effective electrical mode shape, say, $\widehat{\mathbf{\Phi}}_{e,k}$, with associated effective modal characteristics $\widehat{\omega}_{e,k}$ and $\widehat{\zeta}_{e,k}$. With the normalization condition given in Equation (28), this mode shape should thus be

$$\widehat{\mathbf{\Phi}}_{e,k}=\frac{1}{\sqrt{\widehat{\mathbf{b}}_{r\mathbf{k}}\widehat{\mathbf{\Delta}}_{\mathbf{k}}\widehat{\mathbf{c}}_{\mathbf{k}r}}}\widehat{\mathbf{c}}_{\mathbf{k}r}. \tag{30}$$

As shall be shown in Section 3.5, it turns out that the matrices $\mathbf{\Omega}_{e,k}$ and $\mathbf{Z}_{e,k}$ can be tuned to enforce these modal characteristics.

Since the matrix $\widehat{\mathbf{\Delta}}_{e,\mathbf{k}}$ is close to the identity matrix, the normalization condition in Equation (28) indicates that the effective electrical mode shapes are close to be orthogonal. This means that their scalar product with $\widehat{\mathbf{b}}_{r\mathbf{k}}$ and $\widehat{\mathbf{c}}_{\mathbf{k}r}$ can be neglected, i.e., these modes are unobservable and uncontrollable from the perspective of the open-circuit mode. Furthermore, the evaluation of Equation (29) at $s=0$ pre- and postmultiplied by $\widehat{\mathbf{b}}_{r\mathbf{k}}$ and $\widehat{\mathbf{c}}_{\mathbf{k}r}$, respectively, reveals that

$$\widehat{\mathbf{b}}_{r\mathbf{k}}\widehat{\mathbf{\Phi}}_{e,k}\widehat{\mathbf{\Phi}}_{e,k}^T\widehat{\mathbf{c}}_{\mathbf{k}r}=\widehat{\mathbf{b}}_{r\mathbf{k}}\widehat{\mathbf{\Delta}}_{\mathbf{k}}^{-1}\widehat{\mathbf{c}}_{\mathbf{k}r}. \tag{31}$$

Under this design choice, the system behaves like the single-degree-of-freedom case [7]. Indeed, from Equations (27), (29) and (31), the dynamics of the resonant open-circuit modal coordinate are given by

$$\left\{\left(s^2+\omega_{oc,r}^2\right)-\frac{\widehat{\mathbf{b}}_{r\mathbf{k}}\widehat{\mathbf{\Delta}}_{\mathbf{k}}^{-1}\widehat{\mathbf{c}}_{\mathbf{k}r}}{s^2\widehat{\omega}_{e,k}^{-2}+2s\widehat{\zeta}_{e,k}\widehat{\omega}_{e,k}^{-1}+1}\right\}\eta_{oc,r}=\mathbf{\Phi}_{oc,r}^T\mathbf{f}. \tag{32}$$

3.3 Optimal electrical resonance frequencies and damping ratios

It is now possible to tune the the resonance frequencies and damping ratios of the networks with the derived effective characteristics. The effective short-circuit resonance frequency is accurately estimated from Equation (32) and is given by

$$\widehat{\omega}_{sc,r}^2 = \widehat{\omega}_{oc,r}^2 - \widehat{\mathbf{b}}_{r\mathbf{k}}\widehat{\mathbf{\Delta}}_{\mathbf{k}}^{-1}\widehat{\mathbf{c}}_{\mathbf{k}r} \tag{33}$$

and, combined with the effective open-circuit resonance frequency defined by Equation (23), allows for the computation of an MEMCF as

$$\widehat{K}_{c,r\mathbf{k}}^2 = \frac{\widehat{\omega}_{oc,r}^2 - \widehat{\omega}_{sc,r}^2}{\widehat{\omega}_{sc,r}^2}. \tag{34}$$

Using the effective resonance frequency $\widehat{\omega}_{oc,r}$ and the MEMCF in the optimal tuning rule derived by Soltani et al [7, 8], an intermediate parameter given by

$$\widehat{r}_{e,k} = \frac{\sqrt{64 - 16\widehat{K}_{c,r\mathbf{k}}^2 - 26\widehat{K}_{c,r\mathbf{k}}^4} - \widehat{K}_{c,r\mathbf{k}}^2}{8}, \tag{35}$$

is used to compute the optimal electrical resonant frequency and damping ratio as

$$\widehat{\omega}_{e,k} = \sqrt{\frac{3\widehat{K}_{c,r\mathbf{k}}^2 - 4\widehat{r}_{e,k} + 8}{4\widehat{K}_{c,r\mathbf{k}}^2 + 4}}\widehat{\omega}_{oc,r} \tag{36}$$

and

$$\widehat{\zeta}_{e,k} = \frac{\sqrt{27\widehat{K}_{c,r\mathbf{k}}^4 + 80\widehat{K}_{c,r\mathbf{k}}^2 + 64 - 16\widehat{r}_{e,k}\left(4 + 3\widehat{K}_{c,r\mathbf{k}}^2\right)}}{\sqrt{2}\left(5\widehat{K}_{c,r\mathbf{k}}^2 + 8\right)}, \tag{37}$$

respectively. These characteristics may be used to tune the electrical resonance frequency and damping matrices. However, these characteristics may need to be modified beforehand to account for the influence of sampling delays.

3.4 Accounting for sampling delays

It has been shown in [2] that delay-induced instabilities may arise when DVAs implement resonant shunts, and a stabilization procedure was proposed therein. It cannot directly be used with MIMO systems, but the procedure can be adapted to the case of networks if all digital units work with the same sampling rate, which is a reasonable assumption in practice. As shown in [2], the stabilization procedure becomes necessary if the sampling period T_s exceeds a value that can be approximated by

$$T_s \geqslant \frac{\sqrt{6}}{10}\frac{\widehat{K}_{c,r\mathbf{k}}^2}{\widehat{\omega}_{sc,r}^2}. \tag{38}$$

Since Section 3.2 showed that the dynamics of multiple decentralized absorbers is equivalent to the case of a single-degree-of-freedom shunt, the problem can be simplified. Specifically, the stabilization procedure requires to know

the poles of the nominal controlled system. An equivalent dimensionless single-degree-of-freedom dynamic elastance is built as

$$\frac{\widehat{V}_p}{\widehat{q}_p} = -\frac{s^2 + \widehat{\omega}_{sc,r}^2}{s^2 + \widehat{\omega}_{oc,r}^2} \tag{39}$$

with the effective characteristics from Equations (26) and (33). The poles of the closed-loop system are computed by solving

$$1 - \frac{\widehat{V}_p}{\widehat{q}_p} \frac{\widehat{\omega}_{e,k}^2}{s^2 + 2\widehat{\zeta}_{e,k}\widehat{\omega}_{e,k}^2 s} = 0, \tag{40}$$

for s. The resulting roots of this quartic equation are noted p_i ($i \in [1,4]$). They are used to find modification factors δ_ω and δ_ζ given by

$$\begin{bmatrix} \delta_\zeta \\ \delta_\omega \end{bmatrix} = \begin{bmatrix} -\dfrac{2\widehat{\zeta}_{e,k}\widehat{\omega}_{e,k}}{p_1 + 2\widehat{\zeta}_{e,k}\widehat{\omega}_{e,k}} & -\dfrac{p_1}{p_1 + 2\widehat{\zeta}_{e,k}\widehat{\omega}_{e,k}} \\ -\dfrac{2\widehat{\zeta}_{e,k}\widehat{\omega}_{e,k}}{p_2 + 2\widehat{\zeta}_{e,k}\widehat{\omega}_{e,k}} & -\dfrac{p_2}{p_2 + 2\widehat{\zeta}_{e,k}\widehat{\omega}_{e,k}} \\ -\dfrac{2\widehat{\zeta}_{e,k}\widehat{\omega}_{e,k}}{p_3 + 2\widehat{\zeta}_{e,k}\widehat{\omega}_{e,k}} & -\dfrac{p_3}{p_3 + 2\widehat{\zeta}_{e,k}\widehat{\omega}_{e,k}} \\ -\dfrac{2\widehat{\zeta}_{e,k}\widehat{\omega}_{e,k}}{p_4 + 2\widehat{\zeta}_{e,k}\widehat{\omega}_{e,k}} & -\dfrac{p_4}{p_4 + 2\widehat{\zeta}_{e,k}\widehat{\omega}_{e,k}} \end{bmatrix}^\dagger \begin{bmatrix} 1 - \dfrac{1 - e^{-T_s p_1}}{T_s p_1} \\ 1 - \dfrac{1 - e^{-T_s p_2}}{T_s p_2} \\ 1 - \dfrac{1 - e^{-T_s p_3}}{T_s p_3} \\ 1 - \dfrac{1 - e^{-T_s p_4}}{T_s p_4} \end{bmatrix}, \tag{41}$$

where $\dagger$ denotes the Moore-Penrose inverse. The modified parameters $\widetilde{\omega}_{e,k}$ and $\widetilde{\zeta}_{e,k}$ are eventually given by

$$\widetilde{\omega}_{e,k} = \frac{1}{\sqrt{(1 + \delta_\omega)}} \widehat{\omega}_{e,k} \tag{42}$$

and

$$\widetilde{\zeta}_{e,k} = (1 + \delta_\zeta)\, \widehat{\zeta}_{e,k} \tag{43}$$

(see [2] for details).

3.5 Electrical matrices

The matrices $\mathbf{\Omega}_{e,k}$ and $\mathbf{Z}_{e,k}$ can now be tuned to enforce the effective modal characteristics $\widehat{\boldsymbol{\phi}}_{e,k}$, $\widehat{\omega}_{e,k}$ and $\widehat{\zeta}_{e,k}$ for the electrical system in Equation (27). From Equations (28) and (30), it is sought to enforce

$$\left(\widehat{\mathbf{\Delta}}_{\mathbf{k}} - \widehat{\omega}_{e,k}^2 \mathbf{\Omega}_{e,k}^{-2}\right) \widehat{\mathbf{c}}_{\mathbf{k}r} = \mathbf{0}. \tag{44}$$

The unknown elements on the diagonal of $\mathbf{\Omega}_{e,k}^{-2}$ can be gathered in a vector $\boldsymbol{\omega}_{e,k}^{-2}$ (where the exponent -2 has no mathematical meaning but is just used to recall the physical meaning of the elements in this vector), i.e.,

$$\mathbf{\Omega}_{e,k}^{-2} = \mathbf{diag}\left(\boldsymbol{\omega}_{e,k}^{-2}\right). \tag{45}$$

We then note that Equation (44) can equivalently be expressed by

$$\widehat{\omega}_{e,k}^2 \mathbf{diag}\left(\boldsymbol{\omega}_{e,k}^{-2}\right) \widehat{\mathbf{c}}_{\mathbf{k}r} = \widehat{\omega}_{e,k}^2 \mathbf{diag}\left(\widehat{\mathbf{c}}_{\mathbf{k}r}\right) \boldsymbol{\omega}_{e,k}^{-2} = \widehat{\boldsymbol{\Delta}}_{\mathbf{k}} \widehat{\mathbf{c}}_{\mathbf{k}r}. \tag{46}$$

Solving for $\boldsymbol{\omega}_{e,k}^{-2}$,

$$\boldsymbol{\omega}_{e,k}^{-2} = \frac{1}{\widehat{\omega}_{e,k}^2} \mathbf{diag}^{-1}\left(\widehat{\mathbf{c}}_{\mathbf{k}r}\right) \widehat{\boldsymbol{\Delta}}_{\mathbf{k}} \widehat{\mathbf{c}}_{\mathbf{k}r}, \tag{47}$$

and the matrix $\boldsymbol{\Omega}_{e,k}^{-2}$ can be reconstructed with Equation (45). The proportional damping matrix

$$\mathbf{Z}_{e,k} = \widehat{\zeta}_{e,k} \widehat{\omega}_{e,k} \boldsymbol{\Omega}_{e,k}^{-1} \tag{48}$$

makes $\widehat{\zeta}_{e,k}$ the damping ratio associated with that electrical mode.

If sampling delays are to be accounted for, the modified parameters defined in Equations (42) and (43) can be used in place of $\widehat{\omega}_{e,k}$ and $\widehat{\zeta}_{e,k}$ in Equations (47) and (48), respectively.

3.6 Admittance realization

The admittance can be realized with the following state-space model

$$\begin{aligned}
\begin{bmatrix} \dot{\boldsymbol{\eta}}_e \\ \ddot{\boldsymbol{\eta}}_e \end{bmatrix} &= \begin{bmatrix} \mathbf{0} & \mathbf{I} \\ -\boldsymbol{\Omega}_e^2 \left(\mathbf{I} - \boldsymbol{\Phi}_{in}^T \mathbf{D}_{BD} \boldsymbol{\Phi}_{out}\right) & -2\boldsymbol{\Omega}_e \mathbf{Z}_e \end{bmatrix} \begin{bmatrix} \boldsymbol{\eta}_e \\ \dot{\boldsymbol{\eta}}_e \end{bmatrix} + \begin{bmatrix} \mathbf{0} \\ \boldsymbol{\Omega}_e^2 \boldsymbol{\Phi}_{in}^T \end{bmatrix} \mathbf{V}_{in} \\
&= \mathbf{A}_e \begin{bmatrix} \boldsymbol{\eta}_e \\ \dot{\boldsymbol{\eta}}_e \end{bmatrix} + \mathbf{B}_e \mathbf{V}_{in} \\
\mathbf{V}_{out} &= \begin{bmatrix} \mathbf{0} & \boldsymbol{\Phi}_{out} \end{bmatrix} \begin{bmatrix} \boldsymbol{\eta}_e \\ \dot{\boldsymbol{\eta}}_e \end{bmatrix} = \mathbf{C}_e \begin{bmatrix} \boldsymbol{\eta}_e \\ \dot{\boldsymbol{\eta}}_e \end{bmatrix}
\end{aligned} \tag{49}$$

The state-space model in Equation (49), representing the dynamic relation that is to be emulated by the DVAs, can be simplified. This allows, i.a., to reduce the computational burden during real-time operation. When the mode shapes are set with the method presented herein, the matrix $\mathbf{I} - \boldsymbol{\Phi}_{in}^T \mathbf{D}_{BD} \boldsymbol{\Phi}_{out}$ becomes singular. Let $\mathbf{X}_s$ be its kernel, such that

$$\left(\mathbf{I} - \boldsymbol{\Phi}_{in}^T \mathbf{D}_{BD} \boldsymbol{\Phi}_{out}\right) \mathbf{X}_s = \mathbf{0}. \tag{50}$$

Then the matrix $\mathbf{A}_e$ is singular as well because

$$\begin{bmatrix} \mathbf{0} & \mathbf{I} \\ -\boldsymbol{\Omega}_e^2 \left(\mathbf{I} - \boldsymbol{\Phi}_{in}^T \mathbf{D}_{BD} \boldsymbol{\Phi}_{out}\right) & -2\mathbf{Z}_e \boldsymbol{\Omega}_e \end{bmatrix} \begin{bmatrix} \mathbf{X}_s \\ \mathbf{0} \end{bmatrix} = \mathbf{0}. \tag{51}$$

These singular modes are unobservable from the host system's perspective since they are also in the kernel of $\mathbf{C}_e$ and thus need not be kept track of. If $\mathbf{T}_r$ is the matrix spanning the subspace orthogonal to $\begin{bmatrix} \mathbf{X}_s^T & \mathbf{0} \end{bmatrix}^T$, then a reduced state-space model can be built as

$$\mathbf{A}_r = \mathbf{T}_r^T \mathbf{A}_e \mathbf{T}_r, \qquad \mathbf{B}_r = \mathbf{T}_r^T \mathbf{B}_e, \qquad \mathbf{C}_r = \mathbf{C}_e \mathbf{T}_r, \tag{52}$$

and the admittance matrix of the network is finally

$$\mathbf{Z}_{DVA}^{-1}(s) = \mathbf{B}_r \left(s\mathbf{I} - \mathbf{A}_r\right)^{-1} \mathbf{C}_r. \tag{53}$$

When the network is to be emulated by digital units, an equivalent discrete state-space model can be obtained via Tustin's transform.

3.7 Summary of the tuning procedure

To end this section, the proposed tuning procedure is summarized.

1. Identify a model of the structure (Equation (1)): matrices $\mathbf{\Omega}_{oc}$, $\mathbf{B}$, $\mathbf{C}$ and $\mathbf{D}$.
2. Select the modes to be targeted and set the associated weights for each group $\mathbf{W}^{(g)}$.
3. For each group, determine the optimal input and output electrical mode shapes (Equations (15)-(21)).
4. For each targeted mechanical mode,
   (a) Compute the effective characteristics accounting for non-resonant modes (Equation (26)) and the effective MEMCF (Equations (33) and (34)).
   (b) Compute the optimal effective electrical resonance frequency (Equation (36)) and damping ratio (Equation (37)).
   (c) If necessary (Equation (38)), correct the effective electrical resonance frequency and damping ratios to account for sampling delays effect (Equations (40)-(41)).
   (d) Compute the electrical resonance frequency (Equations (47) and (45)) and damping ratio (Equation (48)) matrices.
5. For each group, compute the state-space matrices in their full (Equation (49)) or reduced (Equation (52)) form.

4 Digital vibration absorbers design

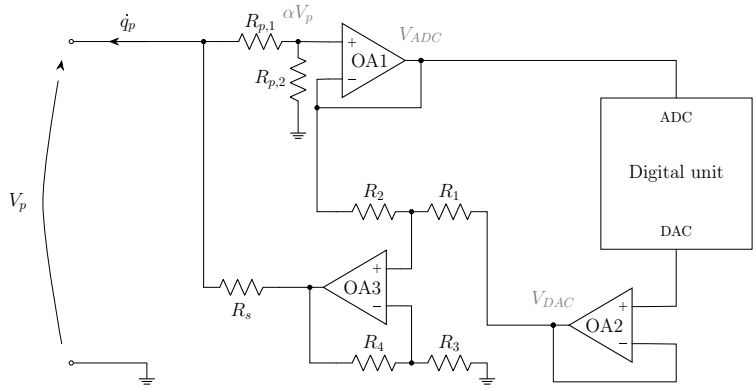

Figure 1: DVA architecture using Howland's current source.

Figure 1 features the architecture of the DVAs used in this work. It is a slight modification of Howland's current source [9, 10], where the resistors labeled $R_{p,1}$ and $R_{p,2}$ have been introduced to attenuate the high piezoelectric voltages in order to avoid saturation of the operational amplifiers (OpAmps). This architecture was favored over the previous one used by the authors (described in [3, 11]) because the latter requires floating piezoelectric electrodes, whereas the version used herein allows for grounding one electrode of each transducer, which was imposed by the experimental setup.

Introducing the division ratio

$$\alpha = \frac{R_{p,2}}{R_{p,1} + R_{p,2}}, \tag{54}$$

the input and output voltages of OA1 are identical and are fed to the analog-to-digital converter (ADC). They are given by

$$V_{ADC} = \alpha V_p. \tag{55}$$

By introducing the amplification gain

$$\beta = 1 + \frac{R_4}{R_3} \tag{56}$$

and the attenuation gain

$$\gamma = \frac{R_1}{R_1 + R_2}, \tag{57}$$

it is possible to show using the ideal OpAmp assumption [9] that the current injected in the load is a function of the digital-to-analog converter (DAC) voltage as well as the load voltage given by

$$\dot{q}_p = \frac{\beta(1-\gamma)}{R_s} V_{DAC} + \frac{(\alpha\beta\gamma - 1)(R_{p,1} + R_{p,2}) - R_s}{R_s(R_{p,1} + R_{p,2})} V_p = g_c V_{DAC} + \delta_c V_p. \tag{58}$$

Ideally, the current should solely be driven by V_{DAC} and thus δ_c should be zero. While the resistances can be adjusted to closely approach $\delta_c = 0$, it is in general not possible to enforce this condition exactly. It is nevertheless possible to counteract this non-ideal behavior by simply modifying the input-output relation implemented in the digital unit. In order to inject the current $\dot{q}_{Id}$, if instead of merely setting $V_{DAC} = \dot{q}_{Id}/g_c$ (which would be the driving law if $\delta_c = 0$), the DAC voltage is given by

$$V_{DAC} = \frac{1}{g_c}\dot{q}_{Id} - \frac{\delta_c}{g_c \alpha} V_{ADC}, \tag{59}$$

then, by Equation (58), the current injected into the load is indeed $\dot{q}_{Id}$ (i.e., $\dot{q}_p = \dot{q}_{Id}$). To determine the parameter $\delta_c/(g_c\alpha)$, a simple test can be carried out when the load is an open circuit ($\dot{q}_p = 0$). Then, by Equations (55) and (58),

$$V_{ADC} = \alpha V_p = -\frac{\alpha g_c}{\delta_c} V_{DAC}. \tag{60}$$

The parameter is thus given by the constant relation between V_{ADC} and V_{DAC} when the load is an open-circuit.

The five DVAs used in this study were all built with identical characteristics. The OpAmps are OPA445 from Texas Instruments [12] and the resistances are given in Table 1.

R_1 (kΩ)	R_2 (kΩ)	R_3 (kΩ)	R_4 (kΩ)	R_s (kΩ)	$R_{p,1}$ (kΩ)	$R_{p,2}$ (kΩ)
10	10	10	115	2.61	49.9	10

Table 1: Resistances of the DVAs used in this study.

References

[1] J. Høgsberg and S. Krenk, "Calibration of piezoelectric RL shunts with explicit residual mode correction," *Journal of Sound and Vibration*, vol. 386, pp. 65–81, 2017. [Online]. Available: http://dx.doi.org/10.1016/j.jsv.2016.08.028

[2] G. Raze, J. Dietrich, and G. Kerschen, "Onset and stabilization of delay-induced instabilities in piezoelectric digital vibration absorbers," *Journal of Intelligent Material Systems and Structures*, p. 1045389X211072269, 2022. [Online]. Available: https://doi.org/10.1177/1045389X211072269

[3] G. Raze, "Piezoelectric digital vibration absorbers for multimodal vibration mitigation of complex mechanical structures," Ph.D. dissertation, Université de Liège, 2021. [Online]. Available: http://hdl.handle.net/2268/256608

[4] G. Raze, J. Dietrich, and G. Kerschen, "Passive control of multiple structural resonances with piezoelectric vibration absorbers," *Journal of Sound and Vibration*, vol. 515, no. August, p. 116490, dec 2021. [Online]. Available: https://linkinghub.elsevier.com/retrieve/pii/S0022460X21005253

[5] J. F. Toftekær and J. Høgsberg, "On the inclusion of structural loading and damping in piezoelectric shunt tuning," *Journal of Sound and Vibration*, vol. 498, p. 115960, apr 2021. [Online]. Available: https://linkinghub.elsevier.com/retrieve/pii/S0022460X21000328

[6] M. Géradin and D. J. Rixen, *Mechanical vibrations: theory and application to structural dynamics*. John Wiley & Sons, 2014. [Online]. Available: https://www.wiley.com/en-us/Mechanical+Vibrations%3A+Theory+and+Application+to+Structural+Dynamics%2C+3rd+Edition-p-9781118900208

[7] P. Soltani, G. Kerschen, G. Tondreau, and A. Deraemaeker, "Piezoelectric vibration damping using resonant shunt circuits: an exact solution," *Smart Materials and Structures*, vol. 23, no. 12, p. 125014, dec 2014. [Online]. Available: http://stacks.iop.org/0964-1726/23/i=12/a=125014?key=crossref.798743ce34b627bed945b046d8a6b51a

[8] T. Ikegame, K. Takagi, and T. Inoue, "Exact Solutions to H_∞ and H_2 Optimizations of Passive Resonant Shunt Circuit for Electromagnetic or Piezoelectric Shunt Damper," *Journal of Vibration and Acoustics*, vol. 141, no. 3, p. 031015, jun 2019. [Online]. Available: https://asmedigitalcollection.asme.org/vibrationacoustics/article/doi/10.1115/1.4042819/727600/Exact-Solutions-to-H-and-H2-Optimizations-of

[9] P. Horowitz and W. Hill, *The Art of Electronics*, 3rd ed. Cambridge University Press, 2015. [Online]. Available: https://artofelectronics.net/

[10] J. Necasek, J. Vaclavik, and P. Marton, "Comparison of analog front-ends for digital synthetic impedance device," in *2017 IEEE International Workshop of Electronics,*

Control, Measurement, Signals and their Application to Mechatronics (ECMSM). IEEE, may 2017, pp. 1–4. [Online]. Available: http://ieeexplore.ieee.org/document/7945916/

[11] A. Fleming, S. Behrens, and S. Moheimani, "Synthetic impedance for implementation of piezoelectric shunt-damping circuits," *Electronics Letters*, vol. 36, no. 18, p. 1525, 2000. [Online]. Available: https://digital-library.theiet.org/content/journals/10.1049/el_20001083

[12] TI, "High Voltage FET-Input Operational Amplifier," 2008. [Online]. Available: https://www.ti.com/product/OPA445